Proceedings of the 26th International Conference on
Port and Ocean Engineering under Arctic Conditions
June 14-18, 2021, Moscow, Russia

Full-scale measurement of ship performance and ice loads in Antarctic floe ice fields

Fang Li[1], Muhammad Bilal Khawar[1], Andrei Sandru[1], Liangliang Lu[1], Mikko Suominen[1], Pentti Kujala[1]
[1] Aalto University, Espoo, Finland

ABSTRACT

Ships going through the polar region often encounter floe ice fields. The interaction between ships and ice floe has received much attention during recent years, resulting in several numerical models developed by various institutes. The Polar Supply and Research Vessel (PSRV) S.A. Agulhas II encountered extensive floe ice fields during its 2018/19 Antarctic voyage. This paper presents the preliminary analysis of the measurement results obtained from this voyage. Ten cases are selected from this voyage, which cover a wide range of ice thickness, floe size and concentration. Information related to ship performance and local ice loads are extracted and their dependences on ice condition and ship maneuvering are identified. In addition, imagery data are processed using a machine vision camera and photogrammetry and image analysis techniques, in order to extract detailed ice floe information in later stage. The findings in this paper provide a general view of ship navigational performance and local ice loads in ice floe fields, and act as a guidance for those who intend to use the data, e.g. for the validation of their simulation models.

KEY WORDS: floe ice; ship resistance; ice loads; machine vision

INTRODUCTION

Ships going through polar regions often encounter floe ice fields, which contain a large amount of ice floes with various thicknesses, shapes and sizes. In reality, a ship goes through an ice floe field by breaking and pushing away the ice floe and/or by avoiding the contact with ice via maneuvering. The performance of a ship and the ice loading on its hull in a floe field thus depend on various parameters involving ice conditions and ship maneuvering.

This paper presents a preliminary analysis of the datasets extracted from ten selected cases of the ship S.A. Agulhas II in floe ice fields during its Antarctic voyage in the southern hemisphere summer of 2018/19. The datasets cover extensive information including ship navigation data, machinery data, ice conditions data and local ice load measurements. The ice conditions datasets cover ice thickness, concentration and floe size, which give an overall view of the ship's performance and ice loading in general floe ice fields. The aim of this paper is to analyze the data in order to identify the dependences between ice conditions, ship maneuvering, resistance and ice loading. This illustrates a general picture of how a ship operates in floe fields and how ship resistance and local loads respond to ice condition in reality. The data will be published along with another paper (Li et al. 2021). Therefore, these analyses will also serve as a reference for the potential users who will use the data to e.g. benchmark their numerical models.

DESCRIPTION OF THE DATASET

The data were collected through the 2018/19 Antarctic voyage of the Polar Supply and Research Vessel (PSRV) S.A. Agulhas II. Figure 1 illustrates the ship route during the 2018/19 voyage. The readers are referred to Lu et al., (2020) for more information about this voyage. The ship is instrumented with shear strain gauges at the starboard side on nine frames, including two at the bow, three at the bow shoulder and four at the stern shoulder (see Figure 2). The measured shear strain is converted to forces according to Suominen et al. (2015). In this paper, the load measurements of the bow and stern shoulder regions will be presented while the bow shoulder measurements are left out because of an instrumentation problem.

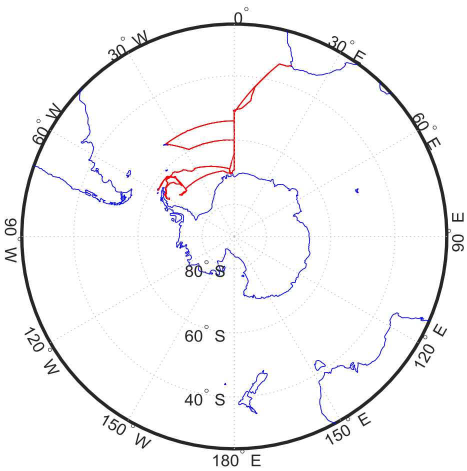

Figure 1. Route of the 2018/19 Antarctic voyage (red) and continents (blue).

Ice conditions during the voyage were monitored via visual observation as well as machine vision. Visual observations were conducted by dedicated ice observers on the bridge, who estimate ice information including concentration, floe size and thickness about every minute, which are then summarized in a ten-minute interval, as described in (Suominen et al., 2016; Suominen et al., 2017). The machine vision estimations were performed via a camera installed on the ship's crow's nest (depicted in Figure 2), which took images of the ice conditions continuously during the voyage. The images were processed offline after the voyage as described in (Sandru et al., 2020), to extract high resolution ice floes information.

To investigate ship resistance and ice loads in ice floe fields, ten cases are selected from the whole voyage for further investigation. The cases are selected to cover a wide range of ice conditions parameters including thickness, concentration and floe size. Criteria of the selection include small variation of ship speed, no major change of ship course, and no obvious drifting of ice floes. Table 1 summarizes the main ice conditions parameters of the selected cases according to visually observed ice conditions. The concentration is a visual estimation of the average ice concentration during each case, while the floe diameter is a visual estimation of the majority ice floe size. Ice thickness is presented in terms of the mean and the maxima because the maxima have major influence on the peak load values. Figure 3 presents examples of orthorectified images (i.e. bird's eye view) of representative photos from the ten selected cases.

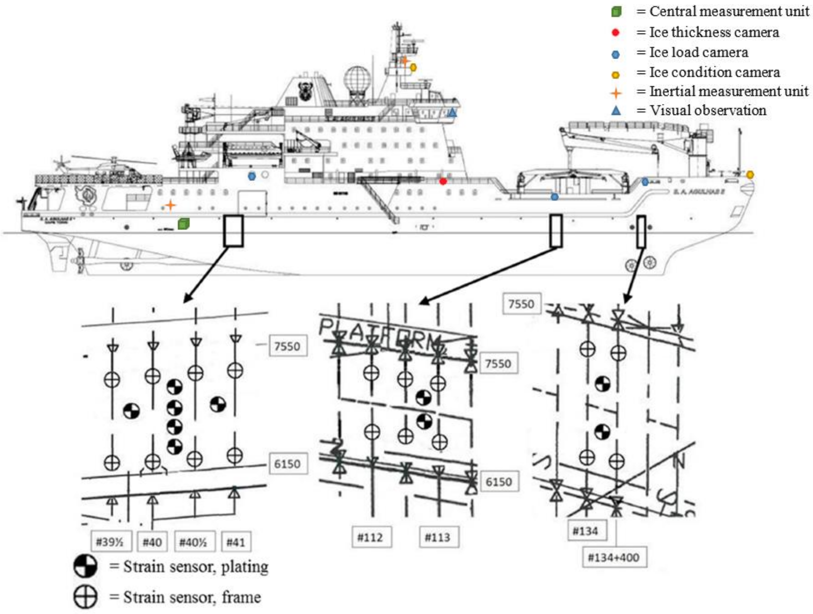

Figure 2. Instrumentation of S.A. Agulhas II

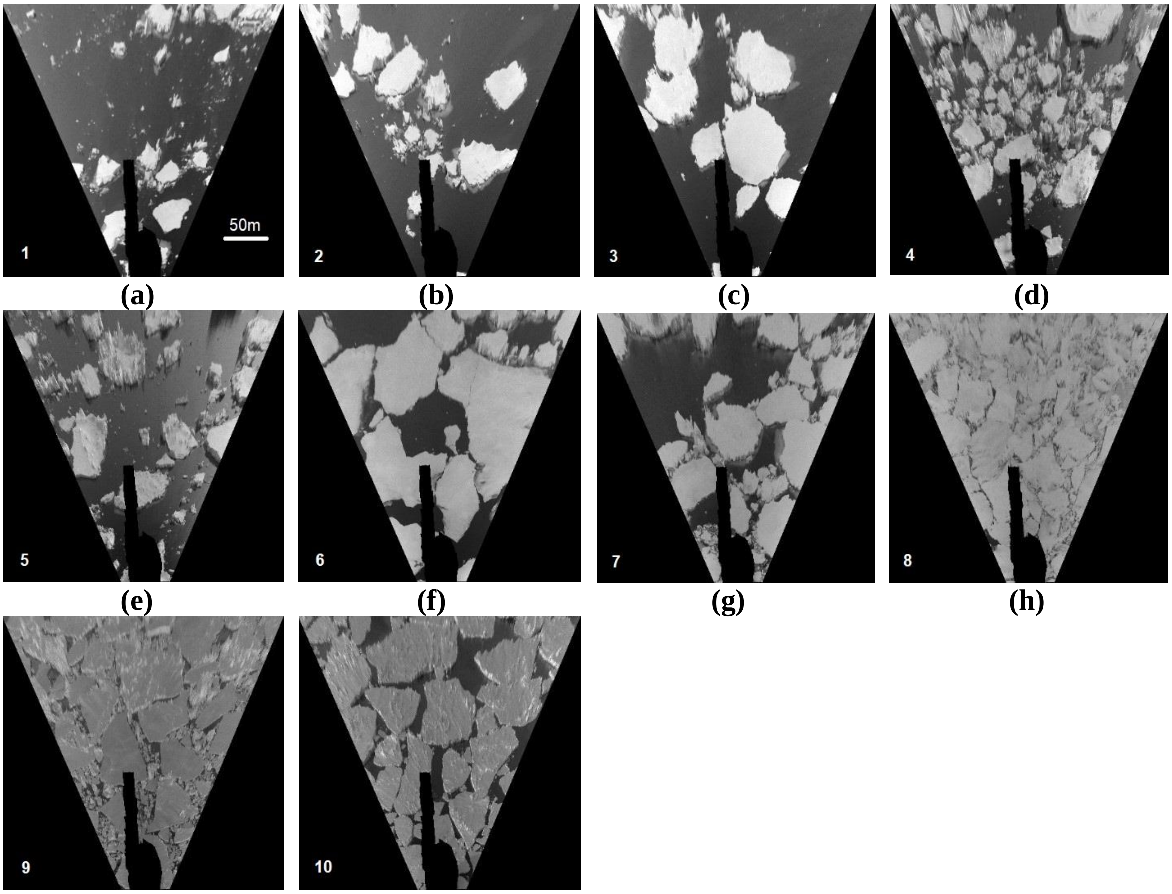

Figure 3. Orthorectified images of representative photos of the selected cases, from (a) to (j) showing case 1 to 10.

Table 1. Summary of the ice conditions parameters for the selected cases

Case	Date	Start time	Duration (min)	h_{mean} (cm)	h_{max} (cm)	Concentration	Floe diameter (m)
1	7-Jan-2019	18:10	28	73	170	30%	0-20m
2	7-Jan-2019	16:40	20	87	110	30%	10-30m
3	8-Jan-2019	09:48	20	72	90	50%	20-50m
4	8-Jan-2019	20:00	30	130	170	50%	0-20m
5	8-Jan-2019	21:08	16	157	225	50%	10-30m
6	6-Jan-2019	09:11	17	56	90	70%	50-100m
7	8-Jan-2019	09:00	20	106	150	70%	20-40m
8	3-Jan-2019	22:01	24	53	110	90%	0-30m
9	3-Jan-2019	20:01	29	72	150	90%	20-50m
10	3-Jan-2019	19:30	30	80	110	90%	20-40m

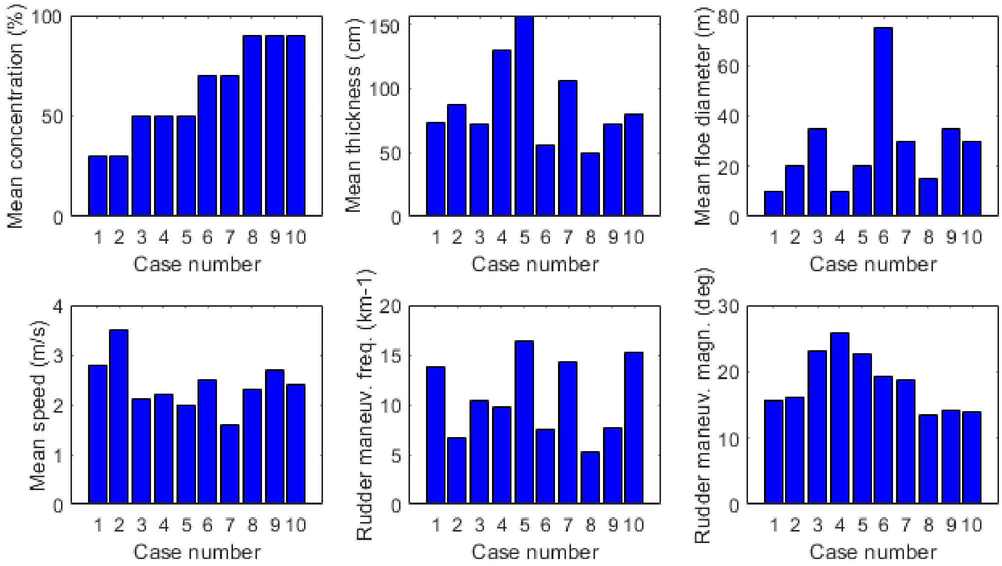

Figure 4. Summary of ice conditions (first row) and ship maneuvering (second row) information of the selected cases.

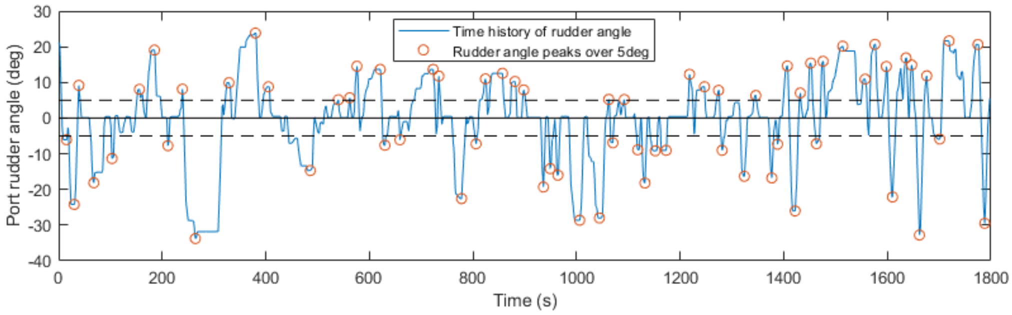

Figure 5. Example of extracting rudder angle peaks from its time history, dashed lines showing the threshold of 5 degrees

Figure 4 summarizes the ice condition parameters and ship maneuvering parameters of the ten selected cases. These are the main factors influencing ship resistance and local ice loads, and will be referred to in later sections to explain the encountered resistance and local loads. To quantify the crew's actions on selecting a course in the floe ice fields, the rudder angle peaks over five degrees are extracted from the time history (Figure 5). The peaks are then summarized in Figure 4 by the occurrence frequency and mean magnitude.

SHIP RESISTANCE

This section looks into the influence of ice conditions and ship speed on ice resistance. The ship thrust measurement is not available so resistance has to be estimated based on the estimation of thrust. Here the revised net thrust model by Li et al. (2018) is used to estimate the net thrust, which is the thrust available to overcome ice resistance. This model is adopted because it takes propeller pitch into account. Propeller pitch varies among these ten cases and has a major influence on the generated thrust. Ship resistance is then estimated simply via Newton's second law:

$$R = T_{net} - ma \tag{1}$$

where R is resistance, T_{net} is the estimated net thrust, m is the mass of the ship and a is the acceleration. Note that here the resistance due to maneuvering of rudder is not considered since it is in a smaller order of magnitude comparing to ice resistance. The propulsion data are published along with Li et al. (2021), so one can make his own estimation of thrust with other method. The aim here is to offer qualitive insight into the resistance as a function of ice condition and ship operation.

Figure 6 presents the calculated mean resistance in these cases. The influence of ice concentration is most evident as the largest resistance all comes from the cases with concentration of 90%. Referring to Figure 4, Influence of ice thickness is also clearly seen as the cases 4 and 5 with thickness over 120cm are featured with relatively large resistance. Conclusions on the influence of floe size cannot be drawn as its influence is not evident. In addition to the ice condition variables, ship speed shows influence on the magnitude of ice resistance. Although with concentration of 70% and thickness of 106cm, case 7 indicates rather small resistance as the result of the lowest speed. The resistance magnitude is only higher than those cases with concentration of 30%. Comparison between cases 4 and 5 indicates some abnormality, as the case with larger thickness does not results in larger resistance. Apart from the possible uncertainty in ice condition data, an explanation can be found by looking into ship maneuvering data. It is found from the time history of rudder angle that in Case 5, the crew maneuvers the ship more often than case 4, probably to avoid major collisions with ice floe since ice floe in case 5 is thicker and larger. The more conservative maneuvering strategy in case 5 may have effectively reduce the resistance.

The above analysis reflects that, ice concentration plays the major role in the encountered resistance magnitude while ice thickness also has clear impact. Influence of ice floe size on resistance cannot be clearly seen. Ship operation, including rudder maneuvering and speed control, also influences the encountered resistance noticeably.

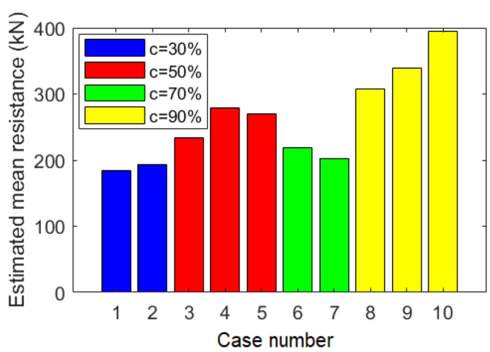

Figure 6. Estimated mean resistance of selected cases

LOCAL ICE LOADS

This section presents local ice loads on the hull. From probabilistic perspective, there are two factors determining the extreme load a ship may encounter during a certain period or distance, e.g. during a voyage or lifetime. The first is the distribution of the individual loads while the second is the exposure, i.e. the number of loads a ship may encounter. Here the aim is to identify the dependence of ice load frequency and load statistics on ice condition and ship operation.

The load data used in this paper are the force data measured with strain gauges. The measured values represent the total ice force on a frame with frame space of 0.4m. The time history of measured ice loads is fed into a Rayleigh separator (Suominen et al., 2015) so that the load peaks can be extracted. An example of the time history if ice loads and the extraction method is given in Figure 7. A threshold of 10kN is adopted since smaller load peaks may contain wave load. Therefore, it should be made clear that the results represent *load peaks over 10kN*. The numbers of loads at bow frames of all cases are mostly over 50, except for that on frame 134.5 of case 5 which has 37 loads. It is then assumed that the number of loads is large enough to support statistical analysis for the bow frames. However, there are much less loads impacting the stern frames. The analysis of stern loads is then only carried out in terms of load frequency.

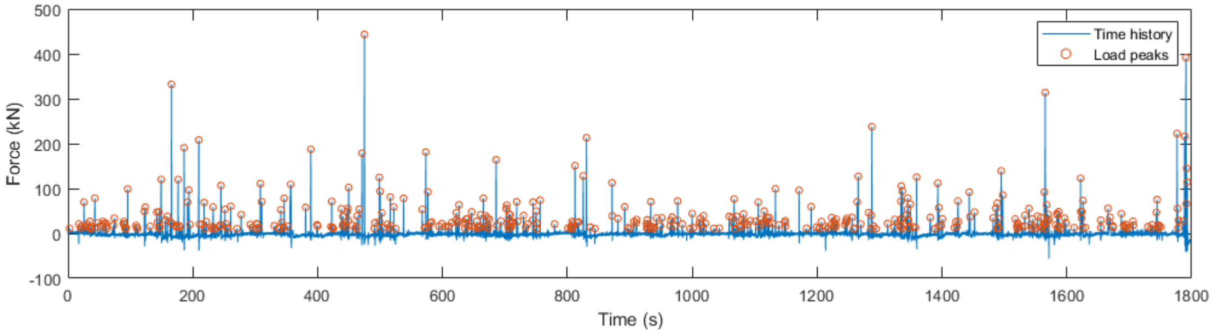

Figure 7. Time history of measure ice loads in case 10 on frame #134.5 and Rayleigh separated load peaks

Load frequency

The number of loads encountered during each case is first analyzed. Since the duration and distance covered by the ten cases are different, the frequency of loads in km^{-1} instead of the total number of loads in each case is calculated for comparison. Figure 8 presents the load frequency on the bow and stern shoulder area as functions of ice condition. The numbers presented here are the mean frequency of loads on the two bow frames. It is clearly shown that the frequency of loading at the bow is majorly determined by ice concentration. The frequency of loading at concentration of 90% is more than twice of those at lower concentrations. Influence of other factors are then in a smaller magnitude comparing to concentration.

Similarly, the figure also indicates the dependence on ice concentration in terms of load frequency at the stern shoulder, but the dependence is much less dominant. There are no loads over 10kN detected with concentration of 30% and 70% but some loads with concentration of 50%. This is due to the fact cases 4 and 5 have rather thick ice, thus more likely resulting in loads over 10kN. It is interesting to see that the loading frequency among the three 90% concentration cases vary significantly, although ice thicknesses are not very different. There must be other reasons leading to the difference. There have been several papers (Valtonen, 2016; Suominen et al., 2020) pointing out the influence of maneuvering on the loading at stern shoulder. Referring to Figure 4, the case with most frequent loading is featured with the most frequent maneuvering among the three cases, which gives evidence to the dependence of loading frequency at stern shoulder on maneuvering.

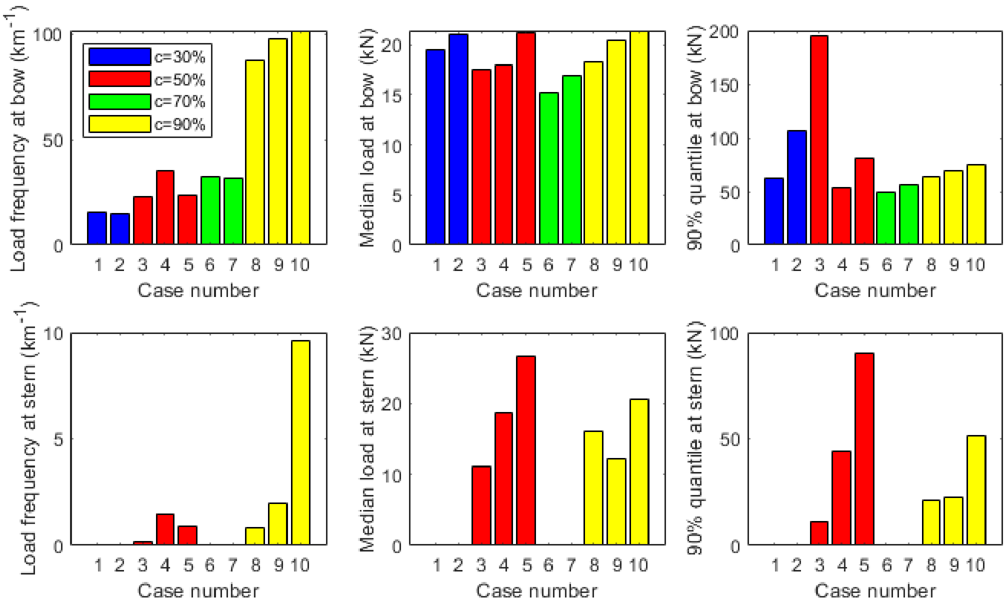

Figure 8. Load frequency and magnitudes of the selected cases

Load magnitude

The next thing to look into are the load magnitude, which is here indicated with median loads and the loads at the 90% quantile, summarized in Figure 8. The maxima are not used because the maximum loads corresponding to different probability of exceedance, as the results of different duration, distance and number of events (i.e. load peaks).

In terms of loads at the bow, unlike resistance as shown in Figure 6, ice concentration shows little effect on the magnitude of the median and 90% quantile. Referring to Figure 4, ice thickness has a clear impact on these two load statistics, by comparing case 1 and 2, 4 and 5, 6 and 7, as well as 8 to 10. The only exception is with case 3, which has relatively thin ice but the highest 90% quantile load, despite that the median is not high. A further investigation into the ice photos of this case demonstrate that the ship met some ridged ice when going through this field, which results in rather large loads comparing to the remaining loads in this case. This explains the very large 90% quantile load. The ridging, however, does not lead to remarkable increase in resistance as shown in Figure 6.

The effect of speed is also evident from cases 2 and 7, with largest and smallest speed respectively. The former has thinner and smaller ice floe but quite large load statistics while the latter is on the contrary. The influence of floe size is also much more evident than that on resistance in Figure 6. This can be seen from Case 4, which has the second thickest ice but smallest ice floe. In this case, the median and 90% quantile are rather small despite of the thick ice. However, the small size of ice floe does not seem to reduce resistance as shown in Figure 6.

The smallest ice load statistics come from the case with the largest ice floe, which may seems abnormal on a first look. Looking into the photos, it can be found that the floe size in this case is so large that the breaking process when going through each floe is similar to level ice, where bending failure constantly happens. In this case the thickness of ice is very low, therefore the large size of ice floe does not lead to high loads because the load magnitude is limited by flexural failure.

The load statistics at the stern shoulder area is also plotted in Figure 8. Due to the small number of loads encountered at the stern shoulder area, there can be large uncertainty associated with the load magnitude statistics. Overall, the dependence on thickness is clearly seen; the dependence on maneuvering seems existing; while dependence on other ice condition factors cannot be drawn here.

To summarize, it can be concluded that ice concentration is the most dominant on the load frequency at the bow while ship maneuvering has a clear effect on the load frequency at stern shoulder. The influence of concentration on load magnitude statistics is not evident. Ice thickness, floe size and ship speed have influence on the load magnitude while their influence on load frequency may be small.

It has been revealed through the previous section and this section that the influence of ice condition and ship maneuvering on the resistance and local ice loads are rather different. This is summarized in Table 2. In this table, 2 denotes that there is strong evidence and the influence is large; 1 denotes that it seems influential but the evidence is not strong; and 0 denotes there is no clear evidence showing its importance based on the current analysis but firm conclusions cannot be made.

Table 2. Summary of the evidence to the influence of ice condition and ship operation on resistance and local loads

	Resistance	Load frequency at bow	Load frequency at stern shoulder	Load magnitude at bow	Load magnitude at stern shoulder
Ice thickness	2	0	1	2	2
Concentration	2	2	2	0	0
Floe size	0	0	0	1	0
Ship speed	2	0	0	2	0
Maneuvering	1	0	2	0	1

IMAGE ANALYSIS OF ICE PHOTOS

Using the techniques described in (Sandru et al., 2020), the raw image is orthorectified (i.e. modified to a bird's eye perspective), thus appearing as if the ice field immediately in front of the ship is looked upon directly from above. Then, a series of orthorectified images are joined together in one single, large image representing the ice field, using a common technique for panorama creation and described next. First, the SURF algorithm (Bay et al., 2008) is used to obtain a series of feature points within each of the orthorectified images. Next, the feature points from two adjacent images are matched, obtaining unique pairs of points, and a transformation matrix (including rotation and translation) is calculated by minimization. The inverse of the aforementioned matrix is used to rectify the second image to overlap the first image, at matching points. Lastly, both images are combined together by overlaying one over another and using a linear metric.

The previously described process is run for a series of images, obtaining a large image of the ice field as presented in Figure 9. Using this approach, the natural movement of the ship is compensated, as long as a suitable base image is selected where the camera angles in world coordinates are known. All the orthorectified images in a series are rectified a second time with respect to the base image.

In the next step, we will analyze the panorama images and extract the floe information for statistical analysis. This will provide high-resolution data which could be later used in comparison with theoretical calculation and numerical simulation results.

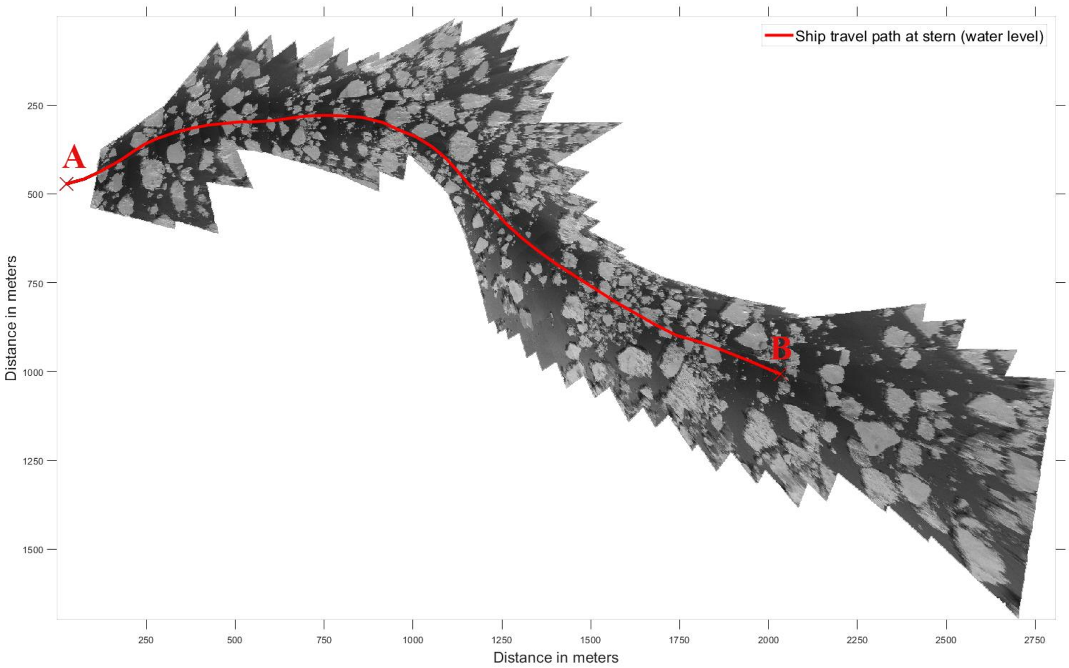

Figure 9. Ice field obtained by stitching a series of orthorectified images. The red line marks the path followed by the ship from beginning (point A) to end (point B), for a total of 14 minutes.

CONCLUSIONS

This paper presents the full-scale measurement results from the Antarctic voyage of S.A. Agulhas II in selected floe ice fields. The influence of ice conditions and ship maneuvering on ship resistance and local ice loads are investigated through analysis of the datasets. It is shown that different factors have different level of influence to the resistance, load frequency and load magnitude at bow and stern regions. The ongoing machine vision analysis work will later provide high-resolution ice data, which enables the possibility to accurately reproduce the ice fields in simulators.

ACKNOWLEDGEMENTS

This project has received funding from the Lloyd's Register Foundation, a charitable foundation, helping to protect life and property by supporting engineering-related education, public engagement and the application of research（www.lrfoundation.org.uk).

REFERENCES

Bay, H., A. Ess, T. Tuytelaars, and L. Van Gool. 2008. “SURF:Speeded Up Robust Features.” Computer Vision and Image Understanding (CVIU). Vol. 110, No. 3, pp. 346–359.

Li, F., Goerlandt, F., Kujala, P., Lehtiranta, J., Lensu, M., 2018. Evaluation of selected state-of-the-art methods for ship transit simulation in various ice conditions based on full-scale measurement. *Cold Regions Science and Technology,* 151, 94–108.

Li, F., Lu, L., Suominen, M., Kujala, P., 2021. Short-term statistics of ice loads on ship bow frames in floe ice fields: full-scale measurements in the Antarctic ocean. Submitted to Marine Structures.

Lu, L., Kujala, P., Banda, O.A.V., Goerlandt, F., 2020. Ramming induced ice loads between the ship bow and multiyear thick ice in Antarctic Weddell sea, in: Developments in the Collision and Grounding of Ships and Offshore Structures - *Proceedings of the 8th International Conference on Collision and Grounding of Ships and Offshore Structures*.

Sandru, A., Hyyti, H., Visala, A., Kujala, P., 2020. A complete process for shipborne sea-ice field analysis using machine vision. In: *International Federation of Automatic Control World Congress*. Berlin, Germany.

Suominen, M., Aalto, H., Kulovesi, J., Lensu, M., Kujala, P., Soal, K., Lehtiranta, J. 2016. Ship-based visual Antarctic sea ice thickness measurements. In: *23nd IAHR International Symposium on Ice*. Ann Arbor, Michigan USA, pp. 1–8.

Suominen, M., Bekker, A., Kujala, P., Soal, K., Lensu, M., 2017. Visual antarctic sea ice condition observations during austral summers 2012-2016. In: *Proceedings of the International Conference on Port and Ocean Engineering under Arctic Conditions*.

Suominen, M., Li, F., Lu, L., Kujala, P., Bekker, A., Lehtiranta, J., 2020. Effect of maneuvering on ice-induced loading on ship hull: Dedicated full-scale tests in the Baltic sea. *Journal of Marine Science and Engineering,* 8, 1–30.

Suominen, M., Romanoff, J., Remes, H., Kujala, P., 2015. The determination of ice-induced loads on the ship hull from shear strain measurements. *Analysis and Design of Marine Structures V*, 375–383.

Valtonen, V., 2016. Effect of Rudder Force on Stern Shoulder Region Ice Loads. In: *Arctic Technology Conference*. pp. 24–26.